Enzyme and Microbial Technology 150 (2021) 109889

Contents lists available at ScienceDirect

Enzyme and Microbial Technology

journal homepage: www.elsevier.com/locate/enzmictec

Hyaluronic acid-coated chitosan nanoparticles as carrier for the enzyme/prodrug complex based on horseradish peroxidase/indole-3-acetic acid: Characterization and potential therapeutic for bladder cancer cells

Fernanda Menezes Pereira [a,b], Micael Nunes Melo [a,b], Átali Kayane Mendes Santos [a,b], Karony Vieira Oliveira [a,b], Fernando Mendonça Diz [c], Rosane Angélica Ligabue [c], Fernanda Bueno Morrone [d], Patrícia Severino [a,b], Alini Tinoco Fricks [a,b,*]

[a] Tiradentes University, Av. Murilo Dantas 300, 49032-490, Aracaju, SE, Brazil
[b] Institute of Technology and Research, Av. Murilo Dantas 300, 49032-490, Aracaju, SE, Brazil
[c] School of Technology, Pontifical Catholic University of Rio Grande do Sul - PUCRS, Av. Ipiranga 6681, 90619-900, Porto Alegre, RS, Brazil
[d] School of Health and Life Sciences, Pontifical Catholic University of Rio Grande do Sul - PUCRS, Av. Ipiranga 6681, 90619-900, Porto Alegre, RS, Brazil

ARTICLE INFO

Keywords:
Hyaluronic acid-coated chitosan nanoparticles
Enzyme/pro-drug therapy
Bladder cancer cells

ABSTRACT

Hybrid nanoparticles composed of different biopolymers for delivery of enzyme/prodrug systems are of interest for cancer therapy. Hyaluronic acid-coated chitosan nanoparticles (CS/HA NP) were prepared to encapsulate individually an enzyme/pro-drug complex based on horseradish peroxidase (HRP) and indole-3-acetic acid (IAA). CS/HA NP showed size around 158 nm and increase to 170 and 200 nm after IAA and HRP encapsulation, respectively. Nanoparticles showed positive zeta potential values (between +20.36 mV and +24.40 mV) and higher encapsulation efficiencies for both nanoparticles (up to 90 %) were obtained. Electron microscopy indicated the formation of spherical particles with smooth surface characteristic. Physicochemical and thermal characterizations suggest the encapsulation of HRP and IAA. Kinetic parameters for encapsulated HRP were similar to those of the free enzyme. IAA-CS/HA NP showed a bimodal release profile of IAA with a high initial release (72 %) followed by a slow-release pattern. The combination of HRP-CS/HA NP and IAA- CS/HA NP reduced by 88 % the cell viability of human bladder carcinoma cell line (T24) in the concentrations 0.5 mM of pro-drug and 1.2 μg/mL of the enzyme after 24 h.

1. Introduction

Bladder cancer (BC) is one of the diseases most frequently related to the urinary tract and is directly associated with a high mortality rate, multiple comorbidities, recurrence episodes and expensive cost of treatment [1,2]. Nanotherapy has been shown to be assertive as strategies in order to improve BC therapy.

Chitosan nanoparticle (CS NP) is considered an excellent alternative for carrying cytotoxic drugs by having biodegradability/biocompatibility, provide controlled release kinetics, low cost and good chemical, physical and biological stability [3–6]. The advantages of using CS NP in cancer therapy, such as reduced side effects and the possibility of action directed to the tumor site, can be maximized with the incorporation of hyaluronic acid (HA) to CS NP [7]. Thus, many studies have been developed in order to investigate hybrid nanoparticles (CS/HA) containing cytotoxic agents for the treatment of several types of cancer [8–14].

HA is an anionic polymer capable of interacting electrostatically with chitosan (cationic structure). It is abundantly present in many living beings [7,15–17]. HA is non-immunogenic and highly soluble in water. Nanoparticles containing HA have longer circulation time, which improve the directing to the tumor area [18,19]. Also, HA interacts with the cell surface through the CD44 receptor, an important glycoprotein which is commonly over-expressed in several types of tumor cells [7, 20–22].

In addition to nanotechnology, the therapy enzyme/prodrug is considered promising. In this proposal, the cytotoxic asset will only be available after the enzyme-prodrug reaction *in situ*. A classic example of this system is the combination of the vegetable enzyme horseradish peroxidase (HRP) and indole-3-acetic acid (IAA), a substance

* Corresponding author at: Tiradentes University, Av. Murilo Dantas 300, 49032-490, Aracaju, SE, Brazil.
E-mail address: alinitf@yahoo.com.br (A.T. Fricks).

https://doi.org/10.1016/j.enzmictec.2021.109889
Received 19 March 2021; Received in revised form 8 July 2021; Accepted 29 July 2021
Available online 2 August 2021

responsible for plant growth and development [23]. Studies carried out in cell culture revealed that in the presence of horseradish peroxidase, IAA acts as a pro-oxidant that increases the formation of reactive oxygen species - cytotoxic species recognized by causing of lipid peroxidation and lesions in nucleic acids [23–25]. Oxidative stress caused by the HRP/IAA system forms the basis of the use of this system in cancer therapy [24,26], including bladder cancer [27,28].

In this work, the enzyme/prodrug therapeutic model consisting of HRP and IAA was encapsulated in different hyaluronic acid-coated chitosan nanoparticles (CS/HA NP) as a promising new proposal for bladder cancer therapy.

2. Materials and methods

2.1. Reagents

Horseradish Peroxidase (HRP) Type VI, RZ 3.0, E.C. 1.11.1.7, Indole-3-acetic acid (IAA) ($C_{10}H_9NO_2$) (98 % purity), Chitosan (Medium Molecular Weight, 190−310 kDa), Sodium Tripolyphosphate ($Na_5P_3O_{10}$, 85 %), Hyaluronic acid from *Streptococcus equi* (Mw = 1500 kDa) and MTT (3-(4,5-dimethylthiazol-2-yl)-2,5-diphenyltetrazolium bromide) (5 mg/mL) were purchased from Sigma-Aldrich Co. (St. Louis, USA). Guaiacol ($C_7H_8O_2$), Hydrogen Peroxide (H_2O_2) 30 %, Dibasic sodium phosphate dihydrate ($Na_2HPO_4.2H_2O$), Sodium hydroxide (NaOH), Ethanol (C_2H_5OH), Sodium acetate (CH_3COONa), and Acetic acid ($C_2H_4O_2$) were obtained from Vetec Química. For biological assays, the reagents used were RPMI-1640, fetal bovine serum (FBS), penicillin-streptomycin (10,000 U/mL), amphotericin B (Fungizone®), and 0.5 % trypsin/EDTA solution were obtained from Gibco Laboratories (Carlsbad, USA). All other chemicals and solvents were analytical grade, and solutions were prepared using ultrapure or distilled water.

2.2. Preparation of nanoparticles

Chitosan nanoparticles (CS NP) were prepared by ionotropic gelation method [29] using CS:tripolyphosphate (TPP) ratio of 5:2 (w/w), based on our previous report [30]. Hyaluronic acid-coated chitosan nanoparticles (CS/HA NP) were prepared according to previous literature [31,32]. HA (0.1 mg/mL) (adapted from [31,32]) was dissolved in sodium acetate buffer (100 mM, pH 5.0) and stirred (1200 rpm/30 min). CS NP were added dropwise into a HA solution at a volumetric ratio CS NP:HA of 1:1.

For the preparation of IAA-loaded CS/HA nanoparticles (IAA-CS/HA NP), IAA was added in HA solution and maintained under magnetic stirring for 30 min. IAA loading effect (8.0–80.0 μM) was evaluated. CS NP were dripped in the HA solution (0.1 mg/mL) containing the IAA at volumetric proportion 1:1. For the preparation of HRP-loaded CS/HA nanoparticles (HRP-CS/HA NP), HRP (8.0 μg/mL) was added into the chitosan solution, followed by the crosslinking with TPP [30]. Then, chitosan nanoparticles containing HRP were dripped into the hyaluronic acid solution (0.1 mg/mL) at volumetric proportion of 1:1. All the samples (natural form or lyophilized) were stored at 4 °C.

2.3. Enzyme activity assay

Enzymatic activity (HRP and HRP-CS/HA NP) was measured based on the formation of tetraguaiacol by oxidation of guaiacol at 25 °C in the presence of H_2O_2 [33,34]. One enzyme unit (U) corresponds to the amount of enzyme capable to produce 1 μmol of product/min at 25 °C and pH 6.0. The reactions were monitored at 470 nm using a UV–vis spectrometer Libra S22 (Biochrom).

2.4. Determination of encapsulation efficiency (EE)

Nanoparticles containing HRP or IAA was centrifuged at 10,000 x g (4 °C/1 h). IAA concentration was determined spectrophotometrically (280 nm) [35]. Encapsulation efficiencies (*EE*) for HRP and IAA were calculated according to Eqs. 1 and 2. The IAA encapsulated concentration was obtained by Eq. 3.

$$EE_{HRP} = \frac{Uo - Uf}{Uo} \; x \; 100 \tag{1}$$

$$EE_{IAA} = \frac{\text{IAAo} - \text{IAAf}}{\text{IAAo}} \; x \; 10 \tag{2}$$

$$[IAA]_{encapsulated}(\mu M) = \text{IAAo} - \text{IAAf} \tag{3}$$

Where U_o is units of peroxidase activity offered for encapsulation and U_f is free units of peroxidase presents in the supernatant after centrifugation. IAA_0 is concentration offered for encapsulation, IAA_f is concentration of the prodrug presents in the supernatant after centrifugation.

2.5. Characterization

Dynamic Light Scattering (DLS) technique was used to obtain the mean size and polydispersity index (PDI) of the nanoparticles. Zeta potentials of the nanoparticles were measured by a Malvern Zetasizer Nano S. Scanning electron microscopy (SEM) images were taken using a Inspect F50 microscope (FEI Company) with field emission guns. Liquid samples were dropped on aluminum stubs covered with carbon tape, dried at 40 °C for 2 h, metalized with gold in the secondary electron mode, and then analyzed at 20 kV. Lyophilized nanoparticles and raw materials (HRP, IAA, CS and HA) were analyzed by Fourier-transformed infrared spectroscopy (FTIR) in spectrophotometer Cary 630 (Agilent Technologies), equipped with a zinc selenide crystal (ZnSe) and ATR (total attenuated reflection) device. Thermogravimetric analysis (TGA) was performed in SDT equipment model Q600 (TA Instruments): heating flow 10 °C/min (35 °C–600 °C) under nitrogen atmosphere (10 mL/min). Differential scanning calorimetry (DSC) was performed in DSC-50 cell (Shimadzu): heating flow 10 °C/min (30 °C–500 °C) under nitrogen atmosphere (50 mL/min).

2.6. Determination of kinetic parameters

Kinetic parameters (K_M and V_{max}) of HRP-CS/HA NP were calculated using the values obtained from Lineweaver-Burk plot. Oxidation rates for guaiacol (concentration range 10–100 mM) were obtained using methodology described in the topic 2.3.

2.7. In vitro release of IAA

IAA-CS/HA NP sample (10 mL) - suspension obtained from IAA encapsulation at 80 μM - was placed into a dialysis bag (5 cm length, 25 mm wide and 16 mm in diameter, 14,000 MWCO - InLab) which was immersed in 90 mL of phosphate buffer solution simulating the tumor microenvironment (pH 5.5) at 37 °C, under magnetic stirring (200 rpm). At programmed times (0, 0.5, 1, 2, 3, 6, 9, and 12 h), 1 mL of the release medium was collected, and an equal volume of fresh medium was added. The released IAA in the outside medium was measured by spectrophotometry (280 nm). The cumulative release percentage (CR) of IAA was determined from the Eq. 4:

$$CR = \frac{IAA_t}{IAA_i} \; x \; 100 \tag{4}$$

where IAA_t and IAA_i are the amount of drug released at the time *t* and the initial amount of drug encapsulated in the nanoparticle, respectively.

Release data were analyzed by using different kinetic model equations (zero order, first order, Higuchi's square root plot, Korsmeyer-Peppas, and Hixson-Crowell cube root plot). The diffusion exponent (n), which indicates the release mechanism, was calculated from the

slope of the plot obtained through the Korsmeyer-Peppas model.

2.8. Cytotoxicity assay

Human urinary bladder cancer cell line (T24) (ATCC) was cultured in RPMI medium supplied with 10 % fetal bovine serum (FBS), 0.5 U/mL penicillin/streptomycin at 37 °C in a humidified atmosphere containing 5% CO_2. Then, cells were lifted from the subconfluent cultures with 0.5 % trypsin in 5 mM EDTA. 5000 cells were seeded in 96-well plates and grown for 24 h, followed by treatment with the combination between free HRP (1.2 μg/mL) and IAA (0.1, 0.5 and 1.0 mM), or HRP-CS/HA NP (1.2 μg/mL) and IAA-CS/HA NP (0.1, 0.5 and 1.0 mM) for 24 h. CS/HA NP, HRP-CS/HA NP and IAA-CS/HA NP were carried out individually (positive control) and cells treated only with medium consisted the control experiment for comparative purposes. Considering the encapsulation efficiency of nanoparticles as a correction factor, the appropriate concentrations of HRP and IAA into the nanoparticles were obtained after centrifuging the dispersions at 5000 x *g* and different spin times using an Amicon® Ultra-15 Centrifugal Filter with a molecular weight cutoff of 100 kDa.

Cell viability was evaluated by MTT colorimetric assay [36]. Optical density was measured at 570 nm in automated Victor X3 plate reader (PerkinElmer). Cell viability (%) was calculated as Eq. 5:

$$Cell\ viability = \frac{Absorbance_{sample}}{Absorbance_{control}}\ x\ 100 \quad (5)$$

2.9. Statistical analysis

All experiments were carried out in triplicate and data were presented as the standard error of the mean (mean ± S.E.). The significance level in all statistical analyses was set as a probability of $p < 0.05$. The statistical significance was determined using one-way or two-way ANOVA.

3. Results and discussion

3.1. Particle size, polydispersity index, zeta potential and encapsulation efficiency

The mean size of CS NP was 125.2 ± 0.89 nm and Zeta potential (ZP) value shows a positive charge (+28.53 ± 0.61 mV) due to the presence of protonated amino groups on their surface. Similar results were found by our group [30]. In comparison with CS NP, CS/HA NP showed increasing on mean size (158.3 ± 1.2 nm) and decreasing on positive surface charge (+20.00 ± 0.89 mV). These changes are justified by due to the large volume of the HA chains interacting with the protonated free chitosan clusters on the outside of the NP, resulting in a polyelectrolyte complex [37]. Finally, PDI value for CS NP and CS/HA NP was 0.39 ± 0.01, indicating a relatively homogeneous dispersion of nanoparticles, considering the nature of the constituent of the nanoparticle (a natural polymer - chitosan) [38].

HRP was encapsulated on chitosan nanoparticles coated with HA (HRP-CS/HA NP) with *EE* of 94.29 ± 0.04 %. HRP encapsulation was carried out in two steps pathway: firstly, the cross-linking of the chitosan matrix containing the enzyme with TPP, followed by coating the nanoparticle with HA. This result points to a better efficiency of HRP encapsulation after coating with HA compared with *EE* of HRP on chitosan nanoparticles (65.8 %) [30]. This indicates that the presence of HA plays an important role in HRP encapsulation in biopolymeric nanoparticles. Protein and polysaccharide molecules are able to associate via non-covalent interactions, such as electrostatic and hydrophobic interactions, steric exclusion and hydrogen binding. In fact, electrostatic interactions are predominant considering charged polysaccharides and are especially favored between negatively charged polysaccharides (i.e. hyaluronic acid - COO^-) and positively charged proteins [39]. HRP has a pI of 8.3. Thus, this enzyme has a positive net charge (NH_3^+) at pH 5.0 [40]. The negative charge density along the biopolymer (HA) and its flexibility may be sufficient to conform the charged units of the polymer with the regions positively charged of the enzyme [41], resulting in the high encapsulation efficiency of HRP in CS/HA nanoparticles. The literature exemplifies the most successful loading of positively charged proteins in HA. Loading efficiency of 59.9 % for positively charged lysozyme in HA microgel was observed in literature, while for neutral IgG and negatively charged BSA was 6.5 % and 5.4 %, respectivelly [42].

Fig. 1 shows the effect of IAA loading (8.0–80.0 μM) on the encapsulation in CS/HA NPs. The increase in offered IAA results in a linear increase of encapsulated IAA (solid circles). The EE_{IAA} presented a slight reduction as the IAA concentration was increased (open squares) - from 100 % (8 μM) to 92.36 ± 0.04 % (80 μM). These results indicate that a 10-fold increase in the offered IAA concentration results in an *EE* reduction lower than 10 %, demonstrating that CS/HA NP is able to encapsulate high contents of IAA. In the present proposal, in addition to a high EE, it is desired higher number of encapsulated prodrug molecules. Thus, IAA offered in the concentration of 80 μM was adopted as the optimal loading for obtaining IAA-CS/HA NP.

The high EE_{IAA} values observed for obtaining IAA-CS/HA NP suggests that prodrug was both physically confined in the interstices of the nanostructured material and bound by weak interactions (hydrogen bonding) to the polymeric matrices. IAA can be involved in two different types of hydrogen bonding: N–H•••O and O–H•••O between the NH of the tryptophan moiety of IAA as well as the carbonyl/carboxyl groups with the biopolymers [43]. Also, interactions between the acidic hydrogen of the carboxyl group from IAA and the hydroxyl oxygen of C_6 from chitosan, should be mentioned. In addition, there is a possibility of the hydrogen linked to the pyrrolic nitrogen of IAA interacts weakly also with the hydroxyl oxygen of C_6 from HA in the stabilization phase, before chitosan nanoparticles were dripped in the HA/IAA solution. Once these groups are capable of establishing interactions with the polymeric matrices of HA and CS, these weak interactions reinforce the fixation of IAA to the nanomaterial.

In comparison with CS/HA NP (158.3 ± 1.2 nm), the loaded nanoparticles (HRP-CS/HA NP and IAA-CS/HA NP) exhibited an increase in the mean diameter (200.3 ± 4.36 nm and 170.9 ± 6.11 nm, respectively) indicating HRP immobilization and IAA incorporation in the nanoparticles. The increase of the mean size in chitosan nanoparticles after HRP immobilization is also reported by literature [30].

HRP-CS/HA NP and IAA-CS/HA NP exhibited PDI value of 0.39 ± 0.02 and ZP values of + 24.40 ± 0.90 mV and + 23.37 ± 1.30 mV, respectively. Thus, positive charge referring to the positive amino groups from CS surface was conserved. The reduction in surface charge compared to the chitosan nanoparticle before coating indicates the presence of HA on the particle surface, contributing to the targeting of

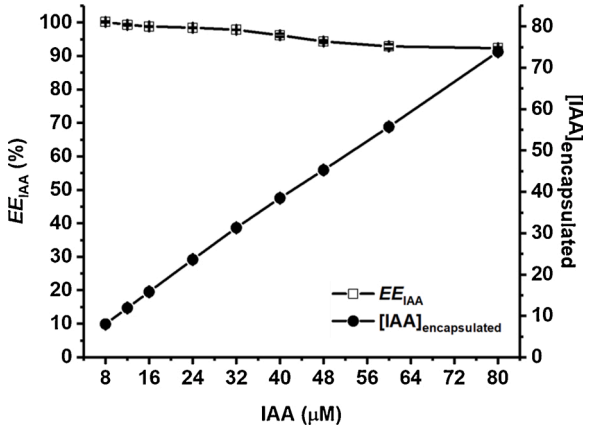

Fig. 1. Effect of IAA loading (8 to 80 μM) on the encapsulation efficiency (%) and encapsulated IAA (μM) for obtaining IAA-CS/HA NP.

CD44 and cell uptake.

The permeable vasculature of tumor tissues allows particles measuring up to 200 nm to passively accumulate due to enhanced permeability and retention effect (EPR) [44]. The particle size for both IAA-CS/HA NP and HRP-CS/HA NP (170 and 200 nm, respectively) may indicate an effective targeting to the cancer tissue once the vascular cut-off in a large range of tumors occurs from 380 to 780 nm [45]. The literature shows penetration and accumulation of HA-based nanoparticles with an average size of 200 nm in the tumor tissue [46]. In addition, the maintenance of the positive surface charge of nanoparticles even with the addition of HA is interesting to cancer therapy once studies have already shown that the electrostatic interaction between the positively charged nanoparticle and the negatively charged plasma membrane of cancer cells is decisive in the internalization of nanoparticles [47]. Furthermore, the colloidal stability of the particles depends directly on their surface charge, indicating, therefore, that particles with a charge between +20 mV and +30 mV are moderately stable [48]. PDI values below 0.5 indicates the formation of relatively homogeneous dispersions of nanoparticles based on natural polymers [49]. Thus, considering mean size, ZP, and PDI values, both HRP and IAA-CS/HA nanoparticles present the ideal parameters for application in cancer therapy in terms of physicochemical and biological properties.

3.2. SEM analysis

SEM images showed the majority of spherical, individual and relatively homogeneous (corroborating with the PDI value - 0.39) (Fig. 2).

SEM image of the CS NP (Fig. 2a) shows a size range between 100−140 nm [50]. CS/HA NP, on the other hand, shows a diameter range predominantly around 150 nm (Fig. 2b), indicating that the coating with HA causes a slight increase in the particle size [51]. Fig. 2c shows IAA-CS/HA NP with mean diameter between 158 nm and 185 nm. Fig. 2d exibhits HRP-CS/HA NP with a diameter from 170 nm to 214 nm, suggesting that the encapsulation of the pro-drug and enzyme that promotes an increase in the mean diameter of CS/HA nanoparticles [52]. Also, SEM images confirm that HRP-CS/HA NP and IAA-CS/HA NP are potential candidates for controlled drug delivery systems considering the morphologic characteristic presented and nanometric size near to 200 nm, being appropriate for use in venous chemotherapy [46].

3.3. FTIR spectra

CS spectrum (Fig. 3a) shows absorption band at 3430, 1660, and 1564 cm^{-1}, resulting from the vibration of the stretching of free axial hydroxyl groups (OH), secondary amine and primary amine, respectively, while band at 2900 cm^{-1} is attributed to the C—H stretch vibration [53]. The band at 1556 cm^{-1} is due to the presence of the protonated amine (deacetylation of chitin) [54]. Bands presented at 1426 cm^{-1} and 1376 cm^{-1} are resulting of asymmetric angular deformations of CH_3 and acetamide groups, respectively. Another band at 1150 cm^{-1} is attributed to the elongation of C—O—C β (1 → 4) [55,56].

CS NP spectrum shows a band between 3000 cm^{-1} and 3450 cm^{-1} that is attributed to the stretching vibration of the hydroxyl and amino groups. This band is wider when compared to the spectrum of pure chitosan, indicating strong hydrogen bonds involved in the formation of nanoparticles [57]. Bands at 1564 cm^{-1} corresponds to NH flexion vibration of the amine I (shifted to 1560 cm^{-1}) and the carbonyl stretch of the amide II at 1660 cm^{-1} (shifted to 1654 cm^{-1}), confirming that the groups $-CONH_2$ and $-NH_2$ are involved in the electrostatic interactions with TPP phosphate groups [58]. The spectrum of CS NP also shows

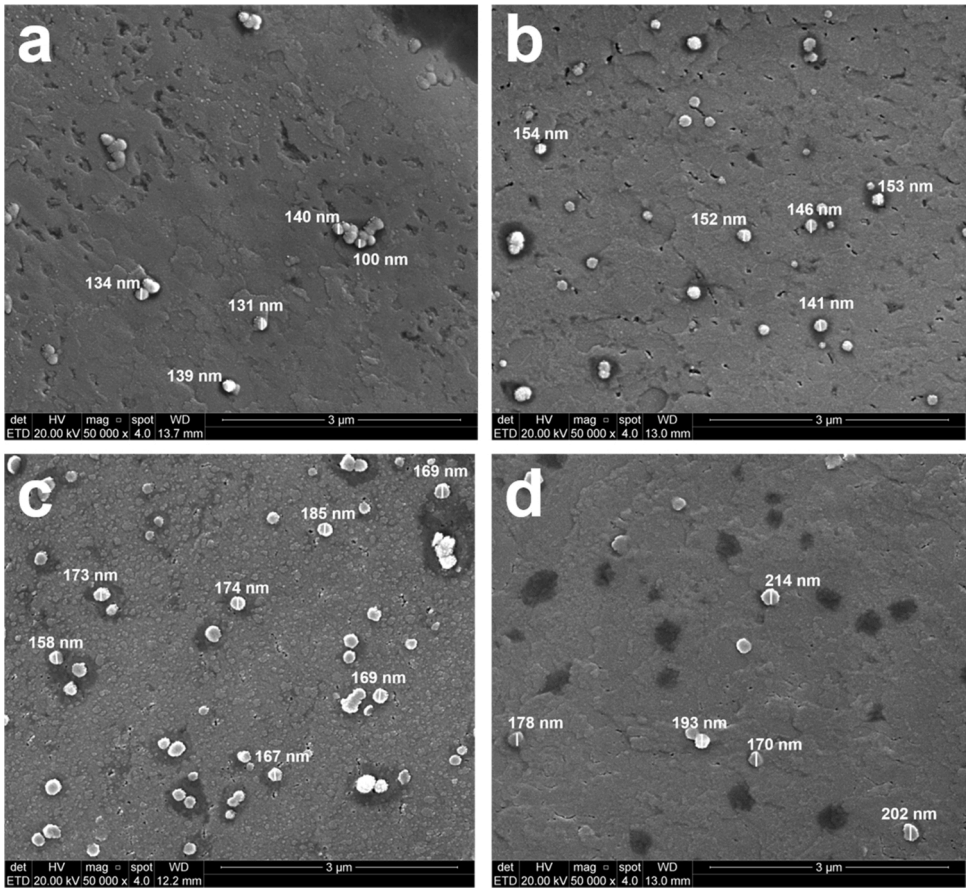

Fig. 2. Micrographs of (a) chitosan nanoparticles (CS NP); (b) hyaluronic acid-coated chitosan nanoparticles (CS/HA NP), (c) hyaluronic acid-coated chitosan nanoparticles containing IAA (IAA-CS/HA NP), and (d) hyaluronic acid-coated chitosan nanoparticles containing HRP (HRP-CS/HA NP).

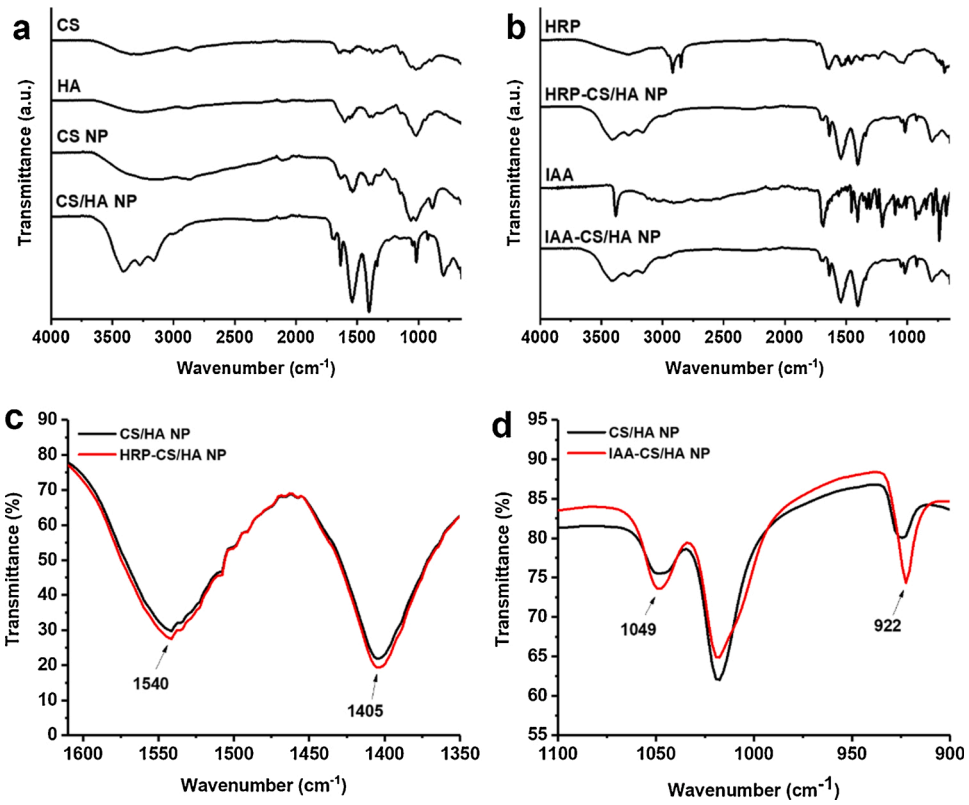

Fig. 3. FTIR spectra of (a) chitosan (CS), hyaluronic acid (HA), chitosan nanoparticles (CS NP), and hyaluronic-coated chitosan nanoparticles (CS/HA NP); and (b) horseradish peroxidase (HRP), hyaluronic acid-coated chitosan nanoparticles containing HRP (HRP-CS/HA NP), indole-3-acetic acid (IAA), and hyaluronic acid-coated chitosan nanoparticles containing IAA (IAA-CS/HA NP); comparison of the FTIR spectra of (c) CS/HA NP and HRP-CS/HA NP between 1610 and 1350 cm^{-1}; and (d) CS/HA NP and IAA-CS/HA NP between 1100 and 900 cm^{-1}.

bands in the range of 1156 cm^{-1} to 1100 cm^{-1} referring to P═O stretching, suggesting the interaction between chitosan and TPP [59].

AH spectrum reveals a characteristic broadband at 3450 cm^{-1} corresponding to the presence of abundant −OH in polysaccharide chains, and band at 1630 cm^{-1}, due to the presence of C═O of the amide [60], and another band at 1415 cm^{-1} corresponding to the C—O connection of the —COONa group [61]. For CS/HA NP spectrum, characteristic bands of HA were observed: a broad and intense band that extends from 2400 cm^{-1} to 3600 cm^{-1} referring to the N—H and O—H stretch vibrations, present in hydrogen bonds. Band at 3100 cm^{-1} is characteristic of the presence of NH [62]. Absorption band around 2900 cm^{-1} is attributed to CH_2 (C—H symmetrical and asymmetric stretching). The extended bands from 1500 cm^{-1} to 1720 cm^{-1} indicate the superposition of the amide I and amide II, as well as C═O from carboxyl. The band at 1560 cm^{-1} in NP QS was shifted to 1540 cm^{-1} in CS/HA NP, pointing to an interaction between the amide groups from chitosan and OH groups from hyaluronic acid [63].

HRP spectrum (Fig. 3b) shows characteristic bands of the protein: 1639 cm^{-1} (amide I) related to α-helix structure, 1540 cm^{-1} (amide II) corresponding to N—H bending and C—N stretching and 1229 cm^{-1} (amide III) related to several modes of NH [64]. IAA spectrum shows a characteristic absorption band at 3389 cm^{-1} assigned to indole ring (N—H) stretching [65]. The bands at 2874 cm^{-1} and 2958 cm^{-1} are attributed to the CH section consisting of asymmetric and symmetric CH_2, respectively. The band at 1690 cm^{-1} corresponds to the carboxylic elongation C═O [66]. The bands observed at 1365 cm^{-1} and 1405 cm^{-1} are attributed to the aromatic vibration of C═C, while bands at 1220 cm^{-1} and 1490 cm^{-1} indicate the presence of CC— elongation. The band at 1100 cm^{-1} corresponds to C–H vibration and the band at 738 cm^{-1} corresponds to the flat deformation of CH_2 [67].

FTIR spectra of the HRP-CS/HA NP and IAA-CS/HA NP nanoparticles were similar to CS/HA NP. The bands corresponding to HRP were overlapped due to the presence of the high intensity bands attributed to the $-COO^-$ group from hyaluronic acid (1405 cm^{-1}) and amine II from chitosan (1540 cm^{-1}), as previously explained. However, a slight increase in these two bands can be observed (Fig. 3c). These changes occur possibly by the overlap with the amide II band from HRP (1540 cm^{-1}) or due to the interactions between those groups from polymers and the enzyme surface.

On the other hand, after the IAA encapsulation, the band at 3389 cm^{-1} attributed to the asymmetric stretching mode of N—H bond of prodrug was concealed by an broad and intense peak produced from the stretching mode of hydrogen-bonded hydroxyl groups in the CS/HA nanoparticles [68]. In addition, an increase of intensity in two regions may be observed to IAA-CS/HA NP with peaks at 922 cm^{-1} and 1049 cm^{-1} (Fig. 3d). These bands are attributed to the modification of −OH from the carboxylic group [69] and the C—OH stretching [70] from IAA, respectively, that may interact with electronegative regions of the polymers, as we propose for the encapsulation model.

3.4. Thermal analysis

Weight loss values as a function of temperature allow to establish the thermal stability of the sample and its decomposition kinetics [71]. TGA and DTG profiles of the CS and nanoparticles can be observed in Fig. 4a and b. CS was degraded in three-stage process. On the first stage (35−100 °C), a weight loss of 10 % referring to removal of water (T_{peak} at 53.23 °C) was observed [72]. The second inflection point occurs at 296 °C and is related to the decomposition of the acetylated and deacetylated units and dehydration of the saccharide rings of the biopolymer, corresponding to around 50 % of the weight loss [63,73]. On the third stage (300−500 °C) was observed a weight loss of about 30 % of the total sample weight and attributed to the chitosan pyrolysis process [74].

Thermogram of CS NP sample reveals that the first stage of the degradation was extended to 200 °C (T_{peaks} at 56 °C and 142 °C) with a loss of 20 % of the total weight, this value was higher than that observed for CS. It is due to the probable increase in the content of free water molecules related to CS NP formation process. Chitosan, like many polysaccharides, has a high affinity for water and tends to be easily

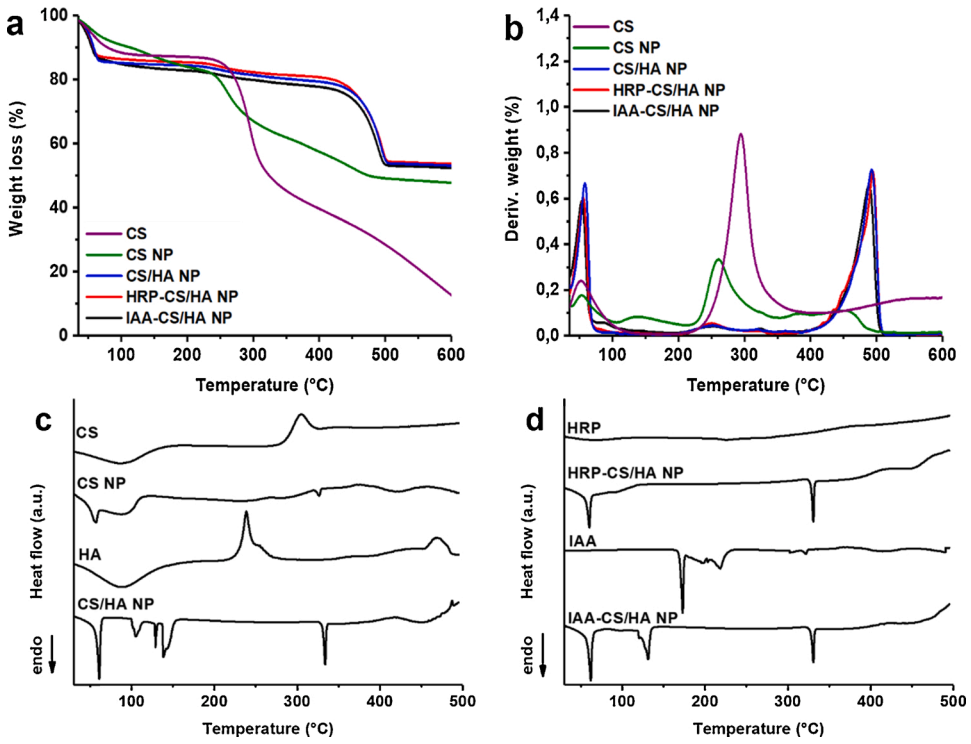

Fig. 4. Thermogravimetric (a) and Derivative Thermogravimetric (b) profiles of chitosan (CS), chitosan nanoparticles (CS NP), hyaluronic acid-coated chitosan nanoparticles (CS/HA NP), hyaluronic acid-coated chitosan nanoparticles containing HRP (HRP-CS/HA NP), and hyaluronic acid-coated chitosan nanoparticles containing IAA (IAA-CS/HA NP); DSC curves of pure nanoparticles and their raw materials (c); and horseradish peroxidase (HRP), indole-3-acetic acid (IAA), and loaded nanoparticles (d).

hydrated [75]. On the second stage of degradation (230−490 °C), where the sample decomposition corresponded to 40 % of the total weight with T_{peak} around 260 °C, dehydration of the saccharide rings and depolymerization of the polymeric units occurs [76]. The decrease in the decomposition temperature of CS NP relative to the chitosan is attributed to the polymer crystallinity loss after solubilization and cross-linking, which becomes an amorphous material and, consequently, reducing its thermal stability [77]. The values of weight loss and TGA profile of CS and CS NP samples were also reported by literature [30].

Thermogravimetric analysis of CS/HA NP shows three thermal events, the first being in the range of 58 °C–200 °C, referring to water loss (30 %) suggesting a higher content of free water and interaction between the chains of HA and CS NP. On the second stage of degradation, as observed with CS NP, a weight loss of 40 % was observed, however with T_{peak} at 492.83 °C [78]. This result indicates the HA coating of the CS NP, possibly by the HA adsorbed on the surface of the CS NP. HA coating causes a delay on the CS/HA NP thermal degradation since the thermal events that signal the depolymerization of the CS/HA NP occurred at a temperature higher than the degradation of the CS NP. Also, CS/HA NP thermogram showed a reduction in the weight loss (20 %) when compared to CS NP (38 %) until 350 °C. This behavior may be attributed to the interactions between chitosan and hyaluronic acid chains that reinforces the structure of CS NP after coating [79]. This result points to an increase in the thermal stability of chitosan nanoparticles after the incorporation of HA, corroborating the literature [80].

Thermograms of the loaded nanoparticles showed similar profiles compared to the pure CS/HA NP. However, HRP-CS/HA NP presents a decomposition event in the range between 200 and 300 °C (T_{peak} at 249 °C), more intense than in pure CS/HA NP. In addition, another event in the range of 400–500 °C (T_{peak} at 494 °C) showed an overall weight loss for HRP-CS/HA NP greater than for pure CS/HA NP (25.22 % and 23.84 %, respectively). Such events may correspond to the thermal degradation of the enzyme. The same was observed by other authors [81,82]. IAA-CS/HA NP thermogram, on the other hand, shows four thermal events at 87 °C (correspond to moisture loss), 145 °C (prodrug thermal decomposition event, as pointed by literature [67]), 252 °C, and 323 °C (both attributed to changes in the chitosan decomposition). In addition, the weight loss observed for IAA-CS/HA NP (22.27 %) is slightly greater when compared to CS/HA NP (20.64 %) until 400 °C. The slight differences in the decomposition temperatures of IAA-CS/HA NP points to the effective loading of the indolic compound. These results are in agreement with reported by the literature [77].

DSC curve of CS (Fig. 4c) shows an endothermic peak at 86 °C (between 70 °C and 130 °C) related to water content associated with the hydrophilic groups of CS. Also, an exothermic peak at 296 °C referring to thermal decomposition of the chitosan pyranose ring was observed. Similar results were reported by literature [72,83]. For CS NP, DSC curve presented endothermic peaks at 57 °C and 282 °C corresponding to dehydration water and breakdown of electrostatic interactions between chitosan and TPP, respectively. Also, an endothermic peak at 330 °C was observed. This peak is attributed to structural changes of the CS due to reticulation process in the nanoparticles synthesis [84].

HA curve shows an endothermic peak at 88 °C attributed to a dehydration event [85]. An exothermic peak also may be exhibited on the HA curve, presenting crystallization around 230 °C [86]. In the CS/HA NP curve, an endothermic peak at 57 °C, also observed in the CS NP curve and attributed to water associated to the biomaterials became sharp, especially by the high hydrophilicity of HA. The coating of CS NP with HA caused the disappearance of the exothermic peak of HA at 230 °C, attributed to the modification of the native structure of HA after the electrostatic interactions with CS [87]. Another endothermic peak of greater intensity (336 °C) compared to the noted in the CS NP curve (330 °C) was observed. This peak assigned to the breakdown of interactions between chitosan and HA [88] also observed the appearance of a peak in this region after the crosslinking of chitosan with alginate, another anionic polymer.

HRP curve presents an endothermic event at 67 °C, attributed to the thermal denaturation of the enzyme (Fig. 4d) [89]. DSC curve of HRP-CS/HA NP shows two endothermic peaks at 59 °C and 330 °C referring to water loss and decomposition of the nanoparticle, respectively, as previously discussed. In addition, the first peak of the HRP-CS/HA NP spectrum presented a different profile to the observed for CS/HA NP, with a melting point followed by decomposition (extended until 123 °C), indicating a superposition between the

dehydration and enzyme denaturation events. This finds suggests an enzyme-nanoparticle interaction and an increase in the thermal stability for HRP after encapsulation [90].

DSC curve of IAA reveals a characteristic and sharp melting point at 171 °C [65]. However, no melting peak of IAA could be detected for the IAA-CS/HA NP formulation. The no detectable endothermic point suggests that the prodrug is present in a molecular dispersion or solid solution state in the polymeric nanoparticles [91]. These results are in agreement with several studies that reported the encapsulation of other drugs using at least one of the polymers evaluated in this study [86, 92–94].

3.5. Kinetic parameters of HRP-CS/HA NP

V_{max} represents the maximum rate of the reaction catalyzed by the enzyme under saturation conditions of substrate, while K_M indicates the substrate concentration that provides half of enzyme maximal activity, representing the degree of enzyme-substrate affinity [95–97]. V_{max} and K_M for HRP-CS/HA NP were calculated using Lineweaver-Burk plot (Fig. 5).

The calculated value of V_{max} for HRP-CS/HA NP was 3.85 ± 0.02 mM/min. This value is lower than that reported in the literature for free HRP using guaiacol as substrate (5.07 ± 0.11 mM/min) [30]. The authors also observed a reduction of 24.6 % on V_{max} after encapsulating HRP in chitosan nanoparticles. It is known that immobilization process of an enzyme can promote conformational changes in its structure [98]. Thus, after immobilization, the reduction on the V_{max} value of the enzyme is observed with frequency in literature [99–103].

Enzymes can lose some of their catalytic properties after being immobilized in different kinds of matrix, as the apparent K_M values of immobilized enzymes became higher than those for free enzymes [104]. Other works have also demonstrated the maintenance of K_M after HRP immobilization [105–108]. In contrast, previous work involving HRP immobilization on different nanoparticles for potential application in cancer therapy demonstrated K_M values notably higher to that of the free enzyme [109,110]. The apparent K_M for HRP-CS/HA NP was 17.29 ± 0.19 mM, similar value than that reported in the literature for free HRP (17.78 ± 0.68 mM) [30], suggesting that enzyme-substrate affinity was not affected after encapsulation.

An important parameter must be considered in enzyme immobilization: diffusion constant (K_α - defined as V_{max} /K_M ratio). For free HRP this value is 0.27 ± 0.02 min^{-1} [30], while for HRP-CS/HA NP this value was 0.22 ± 0.01 min^{-1}, indicating enzyme encapsulation. This behavior occurs due to the limitation in the substrate mass transfer through the reticulated network of chitosan or some possible steric hindrance due to the structural rigidity of the enzymatic structure distorted after encapsulation [103], reducing the guaiacol diffusion to the inside of the nanoparticle.

The results of the kinetic parameters, in special K_M value maintenance, indicate that the application of HRP-CS/HA NP for enzyme/prodrug model presents itself as a suitable resource for anticancer therapeutic studies. HRP-CS/HA NP can convert the prodrug into active molecules, regardless of the release of HRP from the nanoparticle.

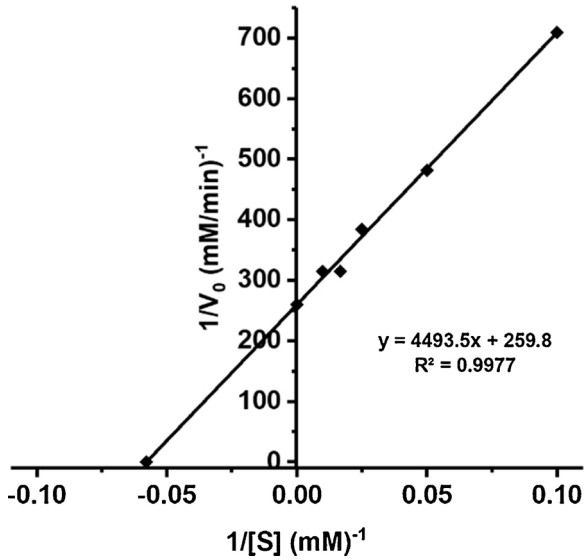

Fig. 5. Lineweaver-Burk plot of HRP-CS/HA nanoparticles.

3.6. In vitro release study for IAA

In order to study the prodrug (IAA) release profile from IAA-CS/HA NP, *in vitro* release test was carried out with maximum time duration of 12 h at pH 5.5 in order to mimic the tumor microenvironment (Fig. 6). The release profile of IAA revealed a biphasic characteristic based on an initial and rapid release phase followed by a sustained release [111]. In the first 3 h the drug release in order of 72 % was observed. This value increases to 88 % after 12 h of testing. According to this result, the literature reports the release profile of heteronemin (a natural marine compound) from HA nanoparticles and also observed a relatively fast and steady pattern in the initial hours, reaching ~73 % after 6 h, and ~90 % after 24 h of incubation [112]. In other study, curcumin was encapsulated in chitosan nanoparticles coated with hyaluronic acid and PEG. The initial release of curcumin in the first two hours was 19 %, increasing to 80.83 % within 6 h [113]. These results suggest the influence of HA in controlling the release of therapeutic agents from nanoparticles.

Table 1 shows the release model analysis of IAA-CS/HA NP based on *in vitro* release experiment data. Zero-order kinetics means that the release of an active agent is governed as a function of time at a constant rate independent of its concentration. Drug dissolution occurs from dosage forms that do not disaggregate and release the drug slowly. This relationship is commonly found in drug delivery systems such as transdermal slow release matrix, coated, and osmotic systems [114]. Thus, it is considered that the zero-order kinetic is not suitable as a release model for IAA-CS/HA NP. First-order release kinetics points that the amount of drug released is proportional to the amount of remaining drug in the matrix and decreasing over time - the amount of active released tends to decrease in function of time. Soluble active agents incorporated into a porous matrix generally provide first-order release kinetics [114]. Considering IAA is sparingly soluble in aqueous solution, first-order kinetics is also not suitable as a release model for IAA-CS/HA

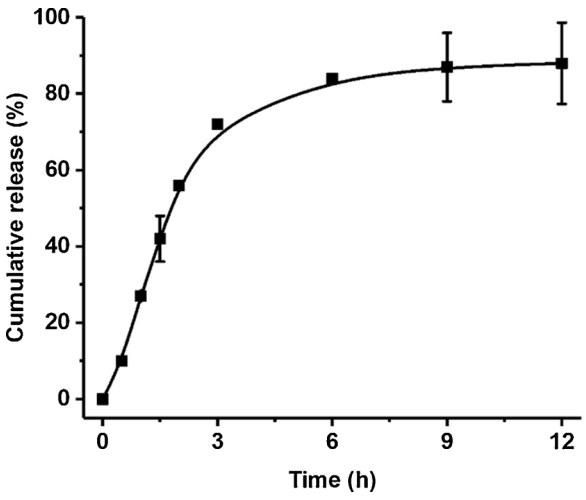

Fig. 6. Cumulative release profile for IAA-CS/HA NP at pH 5.5 during 12 h. Data are shown as mean ± SD (n = 3).

Table 1
Release model analysis of IAA-CS/HA NP based on *in vitro* release experiment data*.

Release model	Model equation	R^2 value	*n*-value
Zero order	M_0-$M_t = kt$	0.9822	—
First order	$\ln M_t = \ln M_0 + kt$	0.9892	—
Higuchi's matrix	M_0-$M_t = kt^{1/2}$	0.9144	—
Korsmeyer-Peppas	$\log (M_0$-$M_t) = \log k + n \log t$	0.9825	0.8356
Hixon-Crowell	$M_0^{1/3}$-$M\ t^{1/3} = k_s t$	0.9937	—

* M_0 represents the initial drug amount; M_t indicates the amount of drug remaining at a specific time; k means the rate constant; t refers to the time; n is the diffusion exponent.

NP.

Higuchi's model considers that the solubility and release of the active agent happen through the porosity of the matrix, where no important alteration of matrix structure occurs during its contact with water [114]. Fitting the data obtained to this release model provided a low correlation coefficient ($R^2 = 0.9144$), indicating that changes in the matrix structure in aqueous media should be considered.

Hixson-Crowell equation affirms that the dissolution of the matrix happens in planes parallel to its surface, decreasing proportionally over time while the geometrical form maintains constant. The drug release is limited by dissolution velocity and not by diffusion, which can occur through the polymeric matrix [114]. Hixson-Crowell model appears to be the best fit for IAA release ($R^2 = 0.9937$) indicating the substance is released from the surface reducing the size is proportionally and maintaining the geometric shape [115]. Thus, IAA is released when the HA coating is deconstructed over the time of exposure to the acidic environment. The term k_s of the Hixson-Crowell equation represents release constant, which relates surface and volume. For cubic or spherical particles this value is constant if the dissolution is constant over the entire system. If the particles are irregular, this behavior is different and a deviation in relationship to values theoretically provided through equation appears [114]. Thus, Hixson-Crowell model for IAA release corroborates the results obtained in the SEM analysis (regular spherical nanoparticles - Fig. 2c).

Korsmeyer-Peppas model describes the drug release from polymeric systems when the release mechanism is not known or when more than one type of phenomenon of drug release is involved, usually matrix relaxation and drug diffusion. In this model also fraction of drug released at time and release rate constant, must be considered the release exponent (*n*-value) [116]. The n value is used to characterize different release for cylindrical shaped matrices. For the case of cylindrical tablets, $0.45 \leq n$ corresponds to a Fickian diffusion mechanism, $0.45 < n < 0.85$ to non-Fickian transport (anomalous transport for spherical geometry), $n = 0.89$ to Case II (relaxational) transport, and $n > 0.89$ to super case II transport [114]. In anomalous transport, there is simultaneously diffusion and relaxation of the polymeric wall or the erosion of the particle as responsible for the release [88]. IAA-CS/HA NP exhibited release by anomalous transport ($n = 0.8356$) for spherical geometric shape - according to the SEM results (Fig. 2c) - and being in agreement with release kinetics profile (rapid release of IAA in the initial hours). The nanoparticle is swollen by the diffusion of the solvent and simultaneously its relaxation and dissolution, releasing IAA. Considering the highly hydrophilic nature of HA, this model is perfectly acceptable for the release of IAA from HA coated chitosan nanoparticles. In addition, the data from release kinetics and the diffusion exponent support the hypothesis that the IAA is physically confined in the interstices of the polymeric matrix and also between the HA layer and the chitosan core of the nanoparticle because weak interactions with the polymers. Thus, the Hixson-Crowell model for IAA release corroborates the results of the DSC and FTIR analysis: no detectable endothermic point of IAA (Fig. 4d), suggesting that the prodrug is present in a molecular dispersion state in the polymeric nanoparticles; and increase in band intensity at 922 cm^{-1} and 1049 cm^{-1} in the FTIR spectrum of IAA-CS/HA NP (Fig. 3d) indicating interactions between IAA and electronegative regions of the polymers.

3.7. Cell viability by MTT assay

The potential of antitumor activity of the combination free (HRP and IAA) or HRP-CS/HA NP and IAA-CS/HA NP was evaluated by MTT assay in human T24 bladder carcinoma cell line after 24 h of exposure (Fig. 7). CS/HA NP, HRP-CS/HA NP and IAA-CS/HA NP, individually tested, did not promote changes in cell viability when compared to the control group. The cytotoxic activity of the prodrug/enzyme systems - free (HRP + IAA) and encapsulated (HRP-CS/HA NP + IAA-CS/HA NP) - showed a cytotoxic effect concentration-dependent. Free HRP (1.2 μg/mL) + IAA at concentrations of 0.1 mM, 0.5 mM, and 1.0 mM provided cell viability of 35 %, 8% and 8%, respectively, showing potent cytotoxic effect of HRP/IAA against T24 bladder carcinoma cells. These results are in agreement with literature: HRP and IAA individually tested did not show cytotoxic activity, while HRP/IAA combination (HRP-1.2 μg/mL and IAA 0.5 mM) reduced the cell viability to less than 20 % [117].

For encapsulated system HRP-CS/HA NP (1.2 μg/mL) combined with IAA-CS/HA NP (0.1 mM, 0.5 mM, and 1.0 mM) the cell viability values observed were 77 %, 33 % and 12 %, respectively. The results show that the cell viability of human T24 bladder carcinoma cell line was statistically equal in the assays with the free (HRP + IAA) and encapsulated (HRP NP + IAA NP) systems at concentration of 1.0 mM. This result is in agreement with the literature. The combined use of free HRP or encapsulated in chitosan nanoparticles at a concentration 1.2 μg/mL and free IAA (100 μM) provided 20 % of cell viability for the human breast cancer cell line (Bcap37) after 36 h [117].

A therapeutic approach involving HRP/IAA guided by chitosan/hyaluronic acid nanoparticles to bladder cancer is promising, since the encapsulated enzyme/prodrug system maintains the therapeutic properties of free biomolecules and presents a high cytotoxic activity in invasive cells. Furthermore, CS/HA NP containing HRP/IAA is advantageous as therapy against tumor cells due to the controled release of IAA in the tumor microenvironment (acidic media), being potentially more effective as a therapeutic model for cancer treatment compared with enzyme/prodrug system in free form.

4. Conclusion

HRP and IAA were encapsulated with high encapsulation efficiencies

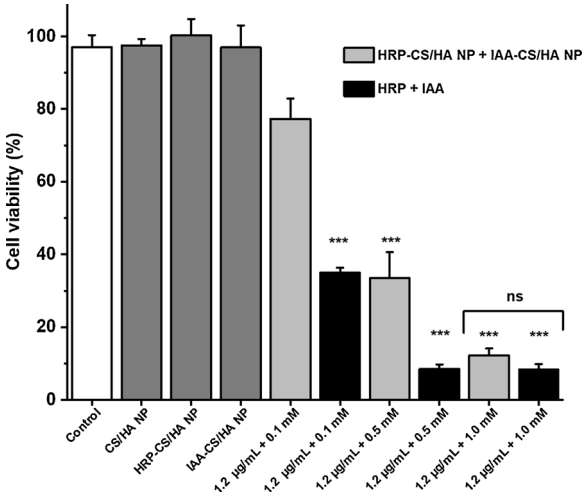

Fig. 7. Cytotoxic effect of Free HRP/IAA and HRP-CS/HA NP (1.2 μg/mL) added to IAA-CS/HA NP in different concentrations (0.1 mM, 0.5 mM, and 1.0 mM) in T24 cell line for 24 h/37 °C. Data were analyzed by one-way ANOVA, followed by Tukey post-hoc. *** $p < 0.001$, ** $p < 0.01$ and * $p < 0.05$.

(94.29 % and 92.36 %, respectively). HRP-CS/HA NP and IAA-CS/HA NP presented particle mean size ≤ 200 nm. Both loaded particles retained a positive surface charge (around +24 mV). SEM analysis showed spherical nanoparticles formation. Physicochemical and thermal characterizations points to the effective encapsulation of molecules. HRP maintains its kinetic parameters after encapsulation in CS/HA nanoparticles. The nanoparticle formulation provided an initial release followed by a gradual and sustained release of IAA in pH 5.5 (88 % in 12 h). The cytotoxic activity of the encapsulated prodrug/enzyme system (HRP-CS/HA NP + IAA-CS/HA NP) was concentration-dependent for T24 cell line and equal to free system (HRP 1.2 μg/mL, IAA 1.0 mM). The combined use of HRP-CS/HA NP and IAA-CS/HA NP is considered promising for bladder cancer therapy.

Author agreement statement

We declare that this manuscript is original, has not been published before and is not currently being considered for publication elsewhere.

We confirm that the manuscript has been read and approved by all named authors and that there are no other persons who satisfied the criteria for authorship but are not listed. We further confirm that the order of authors listed in the manuscript has been approved by all of us.

We understand that the Corresponding Author is the sole contact for the Editorial process.

She is responsible for communicating with the other authors about progress, submissions of revisions and final approval of proofs.

Author contribution section

Fernanda Menezes Pereira: Conceptualization, Methodology, Investigation, Data curation, Writing.

Micael Nunes Melo: Methodology, Investigation, and Writing.

Átali Kayane Mendes Santos, Karony Vieira Oliveira: Methodology and Investigation.

Fernando Mendonça Diz: Investigation and Statistical analysis.

Rosane Angélica Ligabue: Resources, and Writing - Review & Editing.

Fernanda Bueno Morrone: Resources, and Writing - Review & Editing.

Patrícia Severino: Resources, and Writing - Review & Editing.

Alini Tinoco Fricks: Supervision, Conceptualization, Resources, Project administration, Funding acquisition, Writing - Review & Editing.

Declaration of Competing Interest

The authors report no declarations of interest.

Acknowledgements

The Authors are grateful for the financial support from the Brazilian research funding agencies CAPES, CNPq and FAPITEC/SE.

References

[1] M. Burger, J.W.F. Catto, G. Dalbagni, H.B. Grossman, H. Herr, P. Karakiewicz, W. Kassouf, L.A. Kiemeney, C. La Vecchia, S. Shariat, Y. Lotan, Platinum priority – review – bladder cancer epidemiology and risk factors of urothelial bladder cancer, Eur. Urol. 63 (2013) 234–241, https://doi.org/10.1016/j.eururo.2012.07.033.

[2] O.M. Kolawole, W.M. Lau, H. Mostafid, V.V. Khutoryanskiy, Advances in intravesical drug delivery systems to treat bladder cancer, Int. J. Pharm. 532 (2017) 105–117, https://doi.org/10.1016/j.ijpharm.2017.08.120.

[3] F. Canfarotta, M.J. Whitcombe, S.A. Piletsky, Polymeric nanoparticles for optical sensing, Biotechnol. Adv. 31 (2013) 1585–1599, https://doi.org/10.1016/j.biotechadv.2013.08.010.

[4] C.J. Cheng, G.T. Tietjen, J.K. Saucier-Sawyer, W.M. Saltzman, A holistic approach to targeting disease with polymeric nanoparticles, Nat. Rev. Drug Discov. 14 (2015) 239–247, https://doi.org/10.1038/nrd4503.

[5] D. Liu, F. Yang, F. Xiong, N. Gu, The smart drug delivery system and its clinical potential, Theranostics 6 (2016) 1306–1323, https://doi.org/10.7150/thno.14858.

[6] S. Parveen, R. Misra, S.K. Sahoo, Nanoparticles: A boon to drug delivery, therapeutics, diagnostics and imaging, Nanomedicine Nanotechnology, Biol. Med. 8 (2012) 147–166, https://doi.org/10.1016/j.nano.2011.05.016.

[7] L. Zhong, Y. Liu, L. Xu, Q. Li, D. Zhao, Z. Li, H. Zhang, H. Zhang, Q. Kan, J. Sun, Z. He, Exploring the relationship of hyaluronic acid molecular weight and active targeting efficiency for designing hyaluronic acid-modified nanoparticles, Asian J. Pharm. Sci. 14 (2019) 521–530, https://doi.org/10.1016/j.ajps.2018.11.002.

[8] X. Deng, M. Cao, J. Zhang, K. Hu, Z. Yin, Z. Zhou, X. Xiao, Y. Yang, W. Sheng, Y. Wu, Y. Zeng, Hyaluronic acid-chitosan nanoparticles for co-delivery of MiR-34a and doxorubicin in therapy against triple negative breast cancer, Biomaterials. 35 (2014) 4333–4344, https://doi.org/10.1016/j.biomaterials.2014.02.006.

[9] A. Jain, S.K. Jain, In vitro and cell uptake studies for targeting of ligand anchored nanoparticles for colon tumors, Eur. J. Pharm. Sci. 35 (2008) 404–416, https://doi.org/10.1016/j.ejps.2008.08.008.

[10] R. Lee, Y.J. Choi, M.S. Jeong, Y. Il Park, K. Motoyama, M.W. Kim, S.H. Kwon, J. H. Choi, Hyaluronic acid-decorated glycol chitosan nanoparticles for pH-sensitive controlled release of doxorubicin and celecoxib in nonsmall cell lung cancer, Bioconjug. Chem. 31 (2020) 923–932, https://doi.org/10.1021/acs.bioconjchem.0c00048.

[11] C. Pornpitchanarong, T. Rojanarata, P. Opanasopit, T. Ngawhirunpat, P. Patrojanasophon, Catechol-modified chitosan/hyaluronic acid nanoparticles as a new avenue for local delivery of doxorubicin to oral cancer cells, Colloids Surf. B Biointerfaces 196 (2020), https://doi.org/10.1016/j.colsurfb.2020.111279, 111279.

[12] T. Wang, J. Hou, C. Su, L. Zhao, Y. Shi, Hyaluronic acid-coated chitosan nanoparticles induce ROS-mediated tumor cell apoptosis and enhance antitumor efficiency by targeted drug delivery via CD44, J. Nanobiotechnology 15 (2017) 1–12, https://doi.org/10.1186/s12951-016-0245-2.

[13] B. Xiao, M.K. Han, E. Viennois, L. Wang, M. Zhang, X. Si, D. Merlin, Hyaluronic acid-functionalized polymeric nanoparticles for colon cancer-targeted combination chemotherapy, Nanoscale 7 (2015) 17745–17755, https://doi.org/10.1039/c5nr04831a.

[14] W. Zhang, W. Xu, Y. Lan, X. He, K. Liu, Y. Liang, Antitumor effect of hyaluronic-acid-modified chitosan nanoparticles loaded with siRNA for targeted therapy for non-small cell lung cancer, Int. J. Nanomedicine 14 (2019) 5287–5301, https://doi.org/10.2147/IJN.S203113.

[15] N. Gallo, H. Nasser, L. Salvatore, M.L. Natali, L. Campa, M. Mahmoud, L. Capobianco, A. Sannino, M. Madaghiele, Hyaluronic acid for advanced therapies: promises and challenges, Eur. Polym. J. 117 (2019) 134–147, https://doi.org/10.1016/j.eurpolymj.2019.05.007.

[16] G. Huerta-ángeles, K. Nešporová, G. Ambrožová, L. Kubala, V. Velebný, An effective translation: the development of hyaluronan-based medical products from the physicochemical, and preclinical aspects, Front. Bioeng. Biotechnol. 6 (2018) 1–13, https://doi.org/10.3389/fbioe.2018.00062.

[17] J. Kim, J.Y. Chang, Y.Y. Kim, M.J. Kim, H.S. Kho, Effects of molecular weight of hyaluronic acid on its viscosity and enzymatic activities of lysozyme and peroxidase, Arch. Oral Biol. 89 (2018) 55–64, https://doi.org/10.1016/j.archoralbio.2018.02.007.

[18] A. Almalik, H. Benabdelkamel, A. Masood, I.O. Alanazi, I. Alradwan, M. A. Majrashi, A.A. Alfadda, W.M. Alghamdi, H. Alrabiah, N. Tirelli, A.H. Alhasan, Hyaluronic acid coated chitosan nanoparticles reduced the immunogenicity of the formed protein corona, Sci. Rep. 7 (2017) 1–9, https://doi.org/10.1038/s41598-017-10836-7.

[19] T. Lin, A. Yuan, X. Zhao, H. Lian, J. Zhuang, W. Chen, Q. Zhang, G. Liu, S. Zhang, W. Chen, W. Cao, C. Zhang, J. Wu, Y. Hu, H. Guo, Self-assembled tumor-targeting hyaluronic acid nanoparticles for photothermal ablation in orthotopic bladder cancer, Acta Biomater. 53 (2017) 427–438, https://doi.org/10.1016/j.actbio.2017.02.021.

[20] A. Saneja, D. Nayak, M. Srinivas, A. Kumar, V. Khare, A. Katoch, A. Goswami, R. A. Vishwakarma, S.D. Sawant, P.N. Gupta, Development and mechanistic insight into enhanced cytotoxic potential of hyaluronic acid conjugated nanoparticles in CD44 overexpressing cancer cells, Eur. J. Pharm. Sci. 97 (2017) 79–91, https://doi.org/10.1016/j.ejps.2016.10.028.

[21] Y. Leng, A. Abdullah, M.K. Wendt, S. Calve, Hyaluronic acid, CD44 and RHAMM regulate myoblast behavior during embryogenesis, Matrix Biol. 78–79 (2019) 236–254, https://doi.org/10.1016/j.matbio.2018.08.008.

[22] X. Li, T. Cui, W. Zhang, Z. Zhai, F. Wu, Y. Zhang, M. Yang, W. Zhong, W. Yue, Dopamine-functionalized hyaluronic acid microspheres for effective capture of CD44-overexpressing circulating tumor cells, Colloids Surf. B Biointerfaces 196 (2020), https://doi.org/10.1016/j.colsurfb.2020.111281, 111281.

[23] L.K. Folkes, M.F. Dennis, M.R.L. Stratford, L.P. Candeias, P. Wardman, Peroxidase-catalyzed effects of indole-3-acetic acid and analogues on lipid membranes, DNA, and mammalian cells in vitro, Biochem. Pharmacol. 57 (1999) 375–382, https://doi.org/10.1016/S0006-2952(98)00323-2.

[24] L.K. Folkes, P. Wardman, Oxidative activation of indole-3-acetic acids to cytotoxic species - A potential new role for plant auxins in cancer therapy, Biochem. Pharmacol. 61 (2001) 129–136, https://doi.org/10.1016/S0006-2952(00)00498-6.

[25] M.P. De Melo, T.C. Pithon-Curi, R. Curi, Indole-3-acetic acid increases glutamine utilization by high peroxidase activity-presenting leukocytes, Life Sci. 75 (2004) 1713–1725, https://doi.org/10.1016/j.lfs.2004.03.021.

[26] O. Greco, L.K. Folkes, P. Wardman, G.M. Tozer, G.U. Dachs, Development of a novel enzyme/prodrug combination for gene therapy of cancer: horseradish peroxidase/indole-3-acetic acid, Cancer Gene Ther. 7 (2000) 1414–1420, https://doi.org/10.1038/sj.cgt.7700258.

[27] Y.M. Jeong, H. Li, S.Y. Kim, W.J. Park, H.Y. Yun, K.J. Baek, N.S. Kwon, J. H. Jeong, S.C. Myung, D.S. Kim, Photo-activated 5-hydroxyindole-3-acetic acid induces apoptosis of prostate and bladder cancer cells, J. Photochem. Photobiol. B, Biol. 103 (2011) 50–56, https://doi.org/10.1016/j.jphotobiol.2011.01.011.

[28] O. Spadiut, L. Rossetti, C. Dietzsch, C. Herwig, Purification of a recombinant plant peroxidase produced in Pichia pastoris by a simple 2-step strategy, Protein Expr. Purif. 86 (2012) 89–97, https://doi.org/10.1016/j.pep.2012.09.008.

[29] P. Calvo, C. Remuñán-Lópes, J.L. Vila-Jato, M.J. Alonso, Novel hydrophilic chitosan – polyethylene oxide nanoparticles as protein carriers, J. Appl. Polym. Sci. 63 (1997) 125–132, https://doi.org/10.1002/(sici)1097-4628(19970103)63:1<125::aid-app13>3.0.co;2-4https://doi.org/10.1002/(sici)1097-4628(19970103)63:1<125::aid-app13>3.0.co;2-4.

[30] M.N. Melo, F.M. Pereira, M.A. Rocha, J.G. Ribeiro, F.M. Diz, W.F. Monteiro, R. A. Ligabue, P. Severino, A.T. Fricks, Immobilization and characterization of horseradish peroxidase into chitosan and chitosan / PEG nanoparticles : a comparative study, Process Biochem. 98 (2020) 160–171, https://doi.org/10.1016/j.procbio.2020.08.007.

[31] A. Almalik, R. Donno, C.J. Cadman, F. Cellesi, P.J. Day, N. Tirelli, Hyaluronic acid-coated chitosan nanoparticles: molecular weight-dependent effects on morphology and hyaluronic acid presentation, J. Control. Release 172 (2013) 1142–1150, https://doi.org/10.1016/j.jconrel.2013.09.032.

[32] A. Nasti, N.M. Zaki, P. De Leonardis, S. Ungphaiboon, P. Sansongsak, M. G. Rimoli, N. Tirelli, Chitosan/TPP and chitosan/TPP-hyaluronic acid nanoparticles: systematic optimisation of the preparative process and preliminary biological evaluation, Pharm. Res. 26 (2009) 1918–1930, https://doi.org/10.1007/s11095-009-9908-0.

[33] L.C. Lopes, M.T.M. Barreto, K.M. Gonçalves, H.M. Alvarez, M.F. Heredia, R.O.M. A. de Souza, Y. Cordeiro, C. Dariva, A.T. Fricks, Stability and structural changes of horseradish peroxidase: microwave versus conventional heating treatment, Enzyme Microb. Technol. 69 (2015) 10–18, https://doi.org/10.1016/j.enzmictec.2014.11.002.

[34] T. Hirata, S. Izumi, M. Ogura, T. Yawata, Epoxidation of styrenes with the peroxidase from the cultured cells of Nicotiana tabacum, Tetrahedron 54 (1998) 15993–16003, https://doi.org/10.1016/S0040-4020(98)01007-2.

[35] R. Defez, A. Valenti, A. Andreozzi, S. Romano, M. Ciaramella, P. Pesaresi, S. Forlani, C. Bianco, New insights into structural and functional roles of indole-3-acetic acid (IAA): changes in DNA topology and gene expression in bacteria, Biomolecules. 9 (2019) 1–17, https://doi.org/10.3390/biom9100522.

[36] H. Bahadar, F. Maqbool, K. Niaz, M. Abdollahi, Toxicity of nanoparticles and an overview of current experimental models, Iran. Biomed. J. 20 (2016) 1–11, https://doi.org/10.7508/ibj.2016.01.001.

[37] L. Chen, Y. Zheng, L. Feng, Z. Liu, R. Guo, Y. Zhang, Novel hyaluronic acid coated hydrophobically modified chitosan polyelectrolyte complex for the delivery of doxorubicin, Int. J. Biol. Macromol. 126 (2019) 254–261, https://doi.org/10.1016/j.ijbiomac.2018.12.215.

[38] A. Jain, K. Thakur, G. Sharma, P. Kush, U.K. Jain, Fabrication, characterization and cytotoxicity studies of ionically cross-linked docetaxel loaded chitosan nanoparticles, Carbohydr. Polym. 137 (2016) 65–74, https://doi.org/10.1016/j.carbpol.2015.10.012.

[39] J.M. Rodriguez Patino, A.M.R. Pilosof, Protein-polysaccharide interactions at fluid interfaces, Food Hydrocoll. 25 (2011) 1925–1937, https://doi.org/10.1016/j.foodhyd.2011.02.023.

[40] S.N. Warnakulasuriya, M.T. Nickerson, Review on plant protein–polysaccharide complex coacervation, and the functionality and applicability of formed complexes, J. Sci. Food Agric. 98 (2018) 5559–5571, https://doi.org/10.1002/jsfa.9228.

[41] X. Du, P.L. Dubin, D.A. Hoagland, L. Sun, Protein-selective coacervation with hyaluronic acid, Biomacromolecules. 15 (2014) 726–734, https://doi.org/10.1021/bm500041a.

[42] E. Jooybar, M.J. Abdekhodaie, A. Mousavi, B. Zoetebier, P.J. Dijkstra, Enzymatically crosslinked hyaluronic acid microgels as a vehicle for sustained delivery of cationic proteins, Eur. Polym. J. (2019) 234–243, https://doi.org/10.1016/j.eurpolymj.2019.03.032.

[43] S.N. Barnaby, S.H. Frayne, E.M. Smoak, I.A. Banerjee, Biomimetic fabrication of gold nanoparticles on templated indole-3-acetic acid based nanofibers, Mater. Sci. Eng. C. 31 (2011) 620–628, https://doi.org/10.1016/j.msec.2010.11.027.

[44] B.S. Mahmoud, A.H. Alamri, C. McConville, Polymeric nanoparticles for the treatment of malignant gliomas, Cancers (Basel). 12 (2020) 1–28, https://doi.org/10.3390/cancers12010175.

[45] J. Wang, S. Asghar, L. Yang, S. Gao, Z. Chen, L. Huang, L. Zong, Q. Ping, Y. Xiao, Chitosan hydrochloride/hyaluronic acid nanoparticles coated by mPEG as long-circulating nanocarriers for systemic delivery of mitoxantrone, Int. J. Biol. Macromol. 113 (2018) 345–353, https://doi.org/10.1016/j.ijbiomac.2018.02.128.

[46] R. Liu, W. Xiao, C. Hu, R. Xie, H. Gao, Theranostic size-reducible and no donor conjugated gold nanocluster fabricated hyaluronic acid nanoparticle with optimal size for combinational treatment of breast cancer and lung metastasis, J. Control. Release 278 (2018) 127–139, https://doi.org/10.1016/j.jconrel.2018.04.005.

[47] F. Villanueva-Flores, A. Castro-Lugo, O.T. Ramírez, L.A. Palomares, Understanding cellular interactions with nanomaterials: towards a rational design of medical nanodevices, Nanotechnology. 31 (2020), https://doi.org/10.1088/1361-6528/ab5bc8.

[48] S. Bhattacharjee, DLS and zeta potential - what they are and what they are not? J. Control. Release 235 (2016) 337–351, https://doi.org/10.1016/j.jconrel.2016.06.017.

[49] K.V. Jardim, G.A. Joanitti, R.B. Azevedo, A.L. Parize, Physico-chemical characterization and cytotoxicity evaluation of curcumin loaded in chitosan/chondroitin sulfate nanoparticles, Mater. Sci. Eng. C. 56 (2015) 294–304, https://doi.org/10.1016/j.msec.2015.06.036.

[50] S. Jesus, A.P. Marques, A. Duarte, E. Soares, J.P. Costa, M. Colaço, M. Schmutz, C. Som, G. Borchard, P. Wick, O. Borges, Chitosan Nanoparticles, Shedding light on immunotoxicity and hemocompatibility, Front. Bioeng. Biotechnol. 8 (2020), https://doi.org/10.3389/fbioe.2020.00100.

[51] M.A. Kalam, Development of chitosan nanoparticles coated with hyaluronic acid for topical ocular delivery of dexamethasone, Int. J. Biol. Macromol. 89 (2016) 127–136, https://doi.org/10.1016/j.ijbiomac.2016.04.070.

[52] L. Yang, S. Gao, S. Asghar, G. Liu, J. Song, X. Wang, Q. Ping, C. Zhang, Y. Xiao, Hyaluronic acid/chitosan nanoparticles for delivery of curcuminoid and its in vitro evaluation in glioma cells, Int. J. Biol. Macromol. 72 (2015) 1391–1401, https://doi.org/10.1016/j.ijbiomac.2014.10.039.

[53] H.F.G. Barbosa, D.S. Francisco, A.P.G. Ferreira, É.T.G. Cavalheiro, A new look towards the thermal decomposition of chitins and chitosans with different degrees of deacetylation by coupled TG-FTIR, Carbohydr. Polym. 225 (2019), https://doi.org/10.1016/j.carbpol.2019.115232, 115232.

[54] U. Habiba, T.C. Joo, T.A. Siddique, A. Salleh, B.C. Ang, A.M. Afifi, Effect of degree of deacetylation of chitosan on adsorption capacity and reusability of chitosan/polyvinyl alcohol/TiO2 nano composite, Int. J. Biol. Macromol. 104 (2017) 1133–1142, https://doi.org/10.1016/j.ijbiomac.2017.07.007.

[55] S. Shu, X. Zhang, D. Teng, Z. Wang, C. Li, Polyelectrolyte nanoparticles based on water-soluble chitosan-poly(l-aspartic acid)-polyethylene glycol for controlled protein release, Carbohydr. Res. 344 (2009) 1197–1204, https://doi.org/10.1016/j.carres.2009.04.018.

[56] D. Wang, W. Jiang, Preparation of chitosan-based nanoparticles for enzyme immobilization, Int. J. Biol. Macromol. 126 (2019) 1125–1132, https://doi.org/10.1016/j.ijbiomac.2018.12.243.

[57] Z. Du, J. Liu, T. Zhang, Y. Yu, Y. Zhang, J. Zhai, H. Huang, S. Wei, L. Ding, B. Liu, A study on the preparation of chitosan-tripolyphosphate nanoparticles and its entrapment mechanism for egg white derived peptides, Food Chem. 286 (2019) 530–536, https://doi.org/10.1016/j.foodchem.2019.02.012.

[58] S.F. Hosseini, M.R. Soleimani, M. Nikkhah, Chitosan/sodium tripolyphosphate nanoparticles as efficient vehicles for antioxidant peptidic fraction from common kilka, Int. J. Biol. Macromol. 111 (2018) 730–737, https://doi.org/10.1016/j.ijbiomac.2018.01.023.

[59] J. Antoniou, F. Liu, H. Majeed, J. Qi, W. Yokoyama, F. Zhong, Physicochemical and morphological properties of size-controlled chitosan-tripolyphosphate nanoparticles, Colloids Surfaces A Physicochem. Eng. Asp. 465 (2015) 137–146, https://doi.org/10.1016/j.colsurfa.2014.10.040.

[60] R.A.S. Alatawi, M. Monier, N.H. Elsayed, Preparation of photo-crosslinkable cinnamate modified hyaluronic acid for immobilization of horseradish peroxidase, Process Biochem. 88 (2020) 67–77, https://doi.org/10.1016/j.procbio.2019.10.015.

[61] E. Chiesa, R. Dorati, B. Conti, T. Modena, E. Cova, F. Meloni, I. Genta, Hyaluronic acid-decorated chitosan nanoparticles for CD44-targeted delivery of everolimus, Int. J. Mol. Sci. 19 (2018), https://doi.org/10.3390/ijms19082310.

[62] J. Carneiro, P.M. Döll-Boscardin, B.C. Fiorin, J.M. Nadal, P.V. Farago, J.P. De Paula, Development and characterization of hyaluronic acid-lysine nanoparticles with potential as innovative dermal filling, Brazilian J. Pharm. Sci. 52 (2016) 645–651, https://doi.org/10.1590/S1984-82502016000400008.

[63] A.Z. Bazmandeh, E. Mirzaei, Y. Ghasemi, M.A.J. Kouhbanani, Hyaluronic acid coated electrospun chitosan-based nanofibers prepared by simultaneous stabilizing and coating, Int. J. Biol. Macromol. 138 (2019) 403–411, https://doi.org/10.1016/j.ijbiomac.2019.07.107.

[64] K. Theyagarajan, M. Elancheziyan, P.S. Aayushi, K. Thenmozhi, Facile strategy for immobilizing horseradish peroxidase on a novel acetate functionalized ionic liquid/MWCNT matrix for electrochemical biosensing, Int. J. Biol. Macromol. 163 (2020) 358–365, https://doi.org/10.1016/j.ijbiomac.2020.07.005.

[65] S.S.A. Abidi, Y. Azim, A.K. Gupta, C.P. Pradeep, Cocrystals of indole-3-acetic acid and indole-3-butyric acid: Synthesis, structural characterization and Hirshfeld surface analysis, J. Mol. Struct. 1166 (2018) 202–213, https://doi.org/10.1016/j.molstruc.2018.04.035.

[66] S. Panigrahi, S. Mohanty, C.C. Rath, Characterization of endophytic bacteria Enterobacter cloacae MG00145 isolated from Ocimum sanctum with Indole Acetic Acid (IAA) production and plant growth promoting capabilities against selected crops, S. Afr. J. Bot. 000 (2019) 1–10, https://doi.org/10.1016/j.sajb.2019.09.017.

[67] G. Chitra, D.S. Franklin, S. Guhanathan, Indole-3-acetic acid based tunable hydrogels for antibacterial, antifungal and antioxidant applications, J. Macromol. Sci. Part A Pure Appl. Chem. 54 (2017) 151–163, https://doi.org/10.1080/10601325.2017.1265401.

[68] J.H. Yang, Y.S. Han, M. Park, T. Park, S.J. Hwang, J.H. Choy, New inorganic-based drug delivery system of indole-3-acetic acid-layered metal hydroxide nanohybrids with controlled release rate, Chem. Mater. 19 (2007) 2679–2685, https://doi.org/10.1021/cm070259h.

[69] A.A. Kamnev, A.G. Shchelochkov, Y.D. Perfiliev, P.A. Tarantilis, M.G. Polissiou, Spectroscopic investigation of indole-3-acetic acid interaction with iron(III), J. Mol. Struct. 563–564 (2001) 565–572, https://doi.org/10.1016/S0022-2860(00)00911-X.

[70] L. Bencivenni, A. Margonelli, A. Mariani, A. Pieretti, S. Nunziante Cesaro, Combined FTIR Matrix Isolation and Density Functional Studies of Indole-3-Pyruvic Acid Molecule. Spectroscopic Evidence of Gas-Phase Tautomerism, ISRN Phys. Chem. 2012 (2012) 1–11, https://doi.org/10.5402/2012/243741.

[71] T. Jayaramudu, G.M. Raghavendra, K. Varaprasad, G.V.S. Reddy, A.B. Reddy, K. Sudhakar, E.R. Sadiku, Preparation and characterization of poly(ethylene glycol) stabilized nano silver particles by a mechanochemical assisted ball mill process, J. Appl. Polym. Sci. 133 (2016) 1–8, https://doi.org/10.1002/app.43027.

[72] A.P. Duarte Junior, E.J.M. Tavares, T.V.G. Alves, M.R. de Moura, C.E.F. da Costa, J.O.C. Silva Júnior, R.M. Ribeiro Costa, Chitosan nanoparticles as a modified diclofenac drug release system, J. Nanopart. Res. 19 (2017), https://doi.org/10.1007/s11051-017-3968-6.

[73] M.E.S. Ahmed, H.M. Mohamed, M.I. Mohamed, N.G. Kandile, Sustainable antimicrobial modified chitosan and its nanoparticles hydrogels: synthesis and characterization, Int. J. Biol. Macromol. 162 (2020) 1388–1397, https://doi.org/10.1016/j.ijbiomac.2020.08.048.

[74] I. Corazzari, R. Nisticò, F. Turci, M.G. Faga, F. Franzoso, S. Tabasso, G. Magnacca, Advanced physico-chemical characterization of chitosan by means of TGA coupled on-line with FTIR and GCMS: thermal degradation and water adsorption capacity, Polym. Degrad. Stab. 112 (2015) 1–9, https://doi.org/10.1016/j.polymdegradstab.2014.12.006.

[75] A.R. Dudhani, S.L. Kosaraju, Bioadhesive chitosan nanoparticles: preparation and characterization, Carbohydr. Polym. 81 (2010) 243–251, https://doi.org/10.1016/j.carbpol.2010.02.026.

[76] G. Thandapani, P. Supriya Prasad, P.N. Sudha, A. Sukumaran, Size optimization and in vitro biocompatibility studies of chitosan nanoparticles, Int. J. Biol. Macromol. 104 (2017) 1794–1806, https://doi.org/10.1016/j.ijbiomac.2017.08.057.

[77] A. Valderrama N, C. Jacinto H, J. Lay, Y. Flores E, D. Zavaleta C, A.R. Delfín, Factorial design for preparing chitosan nanoparticles and its use for loading and controlled release of indole-3-acetic acid with effect on hydroponic lettuce crops, Biocatal. Agric. Biotechnol. 26 (2020), https://doi.org/10.1016/j.bcab.2020.101640, 101640.

[78] S. Sagbas Suner, B. Ari, F.C. Onder, B. Ozpolat, M. Ay, N. Sahiner, Hyaluronic acid and hyaluronic acid: sucrose nanogels for hydrophobic cancer drug delivery, Int. J. Biol. Macromol. 126 (2019) 1150–1157, https://doi.org/10.1016/j.ijbiomac.2019.01.021.

[79] T. Kutlusoy, B. Oktay, N.K. Apohan, M. Süleymanoğlu, S.E. Kuruca, Chitosan-co-Hyaluronic acid porous cryogels and their application in tissue engineering, Int. J. Biol. Macromol. 103 (2017) 366–378, https://doi.org/10.1016/j.ijbiomac.2017.05.067.

[80] A. Sionkowska, K. Lewandowska, S. Grabska, B. Kaczmarek, M. Michalska, Physico-chemical properties of three-component mixtures based on chitosan, hyaluronic acid and collagen, Mol. Cryst. Liq. Cryst. 640 (2016) 21–29, https://doi.org/10.1080/15421406.2016.1255501.

[81] J.A. Torres, F.G.E. Nogueira, M.C. Silva, J.H. Lopes, T.S. Tavares, T.C. Ramalho, A.D. Corrêa, Novel eco-friendly biocatalyst: soybean peroxidase immobilized onto activated carbon obtained from agricultural waste, RSC Adv. 7 (2017) 16460–16466, https://doi.org/10.1039/c7ra01309d.

[82] V. Sok, A. Fragoso, Preparation and characterization of alkaline phosphatase, horseradish peroxidase, and glucose oxidase conjugates with carboxylated carbon nano-onions, Prep. Biochem. Biotechnol. 48 (2018) 136–143, https://doi.org/10.1080/10826068.2017.1405025.

[83] Z. Sobhani, S.M. Samani, H. Montaseri, E. Khezri, Nanoparticles of chitosan loaded ciprofloxacin: fabrication and antimicrobial activity, Adv. Pharm. Bull. 7 (2017) 427–432, https://doi.org/10.15171/apb.2017.051.

[84] F. Bande, S.S. Arshad, M. Hair Bejo, S. Abdullahi Kamba, A.R. Omar, Synthesis and characterization of chitosan-saponin nanoparticle for application in plasmid DNA delivery, J. Nanomater. 2015 (2015), https://doi.org/10.1155/2015/371529.

[85] D. Sgorla, A. Almeida, C. Azevedo, É.J. Bunhak, B. Sarmento, O.A. Cavalcanti, Development and characterization of crosslinked hyaluronic acid polymeric films for use in coating processes, Int. J. Pharm. 511 (2016) 380–389, https://doi.org/10.1016/j.ijpharm.2016.07.033.

[86] N. Shabani Ravari, N. Goodarzi, F. Alvandifar, M. Amini, E. Souri, M. R. Khoshayand, Z. Hadavand Mirzaie, F. Atyabi, R. Dinarvand, Fabrication and biological evaluation of chitosan coated hyaluronic acid-docetaxel conjugate nanoparticles in CD44+ cancer cells, DARU, J. Pharm. Sci. 24 (2016) 1–12, https://doi.org/10.1186/s40199-016-0160-y.

[87] R.C. Polexe, T. Delair, Elaboration of stable and antibody functionalized positively charged colloids by polyelectrolyte complexation between chitosan and hyaluronic acid, Molecules. 18 (2013) 8563–8578, https://doi.org/10.3390/molecules18078563.

[88] A.E.S. Pereira, P.M. Silva, J.L. Oliveira, H.C. Oliveira, L.F. Fraceto, Chitosan nanoparticles as carrier systems for the plant growth hormone gibberellic acid, Colloids Surf. B Biointerfaces 150 (2017) 141–152, https://doi.org/10.1016/j.colsurfb.2016.11.027.

[89] B.S. Chang, K.H. Park, D.B. Lund, Thermal inactivation kinetics of horseradish peroxidase, J. Food Sci. 53 (1988) 920–923, https://doi.org/10.1111/j.1365-2621.1988.tb08986.x.

[90] E. Kalaiarasan, T. Palvannan, Removal of phenols from acidic environment by horseradish peroxidase (HRP): aqueous thermostabilization of HRP by polysaccharide additives, J. Taiwan Inst. Chem. Eng. 45 (2014) 625–634, https://doi.org/10.1016/j.jtice.2013.07.003.

[91] A.K. Yadav, A. Agarwal, G. Rai, P. Mishra, S. Jain, A.K. Mishra, H. Agrawal, G. P. Agrawal, Development and characterization of hyaluronic acid decorated PLGA nanoparticles for delivery of 5-fluorouracil, Drug Deliv. 17 (2010) 561–572, https://doi.org/10.3109/10717544.2010.500635.

[92] S. Saremi, F. Atyabi, S.P. Akhlaghi, S.N. Ostad, R. Dinarvand, Thiolated chitosan nanoparticles for enhancing oral absorption of docetaxel: preparation, in vitro and ex vivo evaluation, Int. J. Nanomedicine 6 (2011) 119–128, https://doi.org/10.2147/IJN.S15500.

[93] Y. Song, H. Cai, T. Yin, M. Huo, P. Ma, J. Zhou, W. Lai, Paclitaxel-loaded redox-sensitive nanoparticles based on hyaluronic acid-vitamin E succinate conjugates for improved lung cancer treatment, Int. J. Nanomedicine 13 (2018) 1585–1600, https://doi.org/10.2147/IJN.S155383.

[94] A.M. Elwerfalli, A. Al-Kinani, R.G. Alany, A. Elshaer, Nano-engineering chitosan particles to sustain the release of promethazine from orodispersables, Carbohydr. Polym. 131 (2015) 447–461, https://doi.org/10.1016/j.carbpol.2015.05.064.

[95] G.R. VandeZande, J.M. Olvany, J.L. Rutherford, M. Rasmussen, Enzyme stabilization and immobilization IN series editor, Enzym. Stab. Immobil. 1504 (2017) 165–179, https://doi.org/10.1007/978-1-4939-6499-4.

[96] M. Vitolo, Brief review on enzyme activity, World J. Pharm. Res. 9 (2020) 60–76, https://doi.org/10.20959/wjpr20202-16660.

[97] E.I. Canela, G. Navarro, J.L. Beltrán, R. Franco, The meaning of the Michaelis-Menten constant : K m describes a running title solving a Michaelis-Menten paradox Keywords Cell metabolism ; Enzyme kinetics ; Michaelis Menten ; pre-steady-state kinetics, Syst. Biol. (Stevenage) (2019) 1–16.

[98] S.A. Ahmed, M.A.A. Abdella, G.M. El-Sherbiny, A.M. Ibrahim, A.R. El-Shamy, S. M.M. Atalla, M.E. Hassan, Catalytic, kinetic and thermal properties of free andimmobilized Bacillus subtilis -MK1 α-amylase on Chitosan-magnetic nanoparticles, Biotechnol. Rep. 26 (2020), https://doi.org/10.1016/j.btre.2020.e00443 e00443.

[99] J. Rong, Z. Zhou, Y. Wang, J. Han, C. Li, W. Zhang, L. Ni, Immobilization of horseradish peroxidase on multi-armed magnetic graphene oxide composite: improvement of loading amount and catalytic activity, Food Technol. Biotechnol. 57 (2019) 260–271, https://doi.org/10.17113/ftb.57.02.19.5832.

[100] Y.Q. Almulaiky, R.M. El-Shishtawy, M. Aldhahri, S.A. Mohamed, M. Afifi, W. H. Abdulaal, J.A. Mahyoub, Amidrazone modified acrylic fabric activated with cyanuric chloride: a novel and efficient support for horseradish peroxidase immobilization and phenol removal, Int. J. Biol. Macromol. 140 (2019) 949–958, https://doi.org/10.1016/j.ijbiomac.2019.08.179.

[101] W.H. Abdulaal, Y.Q. Almulaiky, R.M. El-Shishtawy, Encapsulation of HRP enzyme onto a magnetic fe3o4 Np–PMMA film via casting with sustainable biocatalytic activity, Catalysts 10 (2020) 1–14, https://doi.org/10.3390/catal10020181.

[102] B. Yu, H. Cheng, W. Zhuang, C.J. Zhu, J. Wu, H. Niu, D. Liu, Y. Chen, H. Ying, Stability and repeatability improvement of horseradish peroxidase by immobilization on amino-functionalized bacterial cellulose, Process Biochem. 79 (2019) 40–48, https://doi.org/10.1016/j.procbio.2018.12.024.

[103] M. Monier, D.M. Ayad, Y. Wei, A.A. Sarhan, Immobilization of horseradish peroxidase on modified chitosan beads, Int. J. Biol. Macromol. 46 (2010) 324–330, https://doi.org/10.1016/j.ijbiomac.2009.12.018.

[104] M.E.A. Afjeh, R. Pourahmad, B. Akbari-Adergani, M. Azin, Characteristics of glucose oxidase immobilized on magnetic chitosan nanoparticles, Food Sci. Technol. 40 (2020) 68–75, https://doi.org/10.1590/fst.32618.

[105] S. Bocanegra-Rodríguez, N. Jornet-Martínez, C. Molins-Legua, P. Campíns-Falcó, New reusable solid biosensor with covalent immobilization of the horseradish peroxidase enzyme: in situ liberation studies of hydrogen peroxide by portable chemiluminescent determination, ACS Omega 5 (2020) 2419–2427, https://doi.org/10.1021/acsomega.9b03958.

[106] M. Besharati Vineh, A.A. Saboury, A.A. Poostchi, A.M. Rashidi, K. Parivar, Stability and activity improvement of horseradish peroxidase by covalent immobilization on functionalized reduced graphene oxide and biodegradation of high phenol concentration, Int. J. Biol. Macromol. 106 (2018) 1314–1322, https://doi.org/10.1016/j.ijbiomac.2017.08.133.

[107] H. Ikemoto, Q. Chi, J. Ulstrup, Stability and catalytic kinetics of horseradish peroxidase confined in nanoporous SBA-15, J. Phys. Chem. C. 114 (2010) 16174–16180, https://doi.org/10.1021/jp103137e.

[108] M. Altikatoglu Yapaoz, A. Attar, An accomplished procedure of horseradish peroxidase immobilization for removal of acid yellow 11 in aqueous solutions, Water Sci. Technol. (2020) 1–10, https://doi.org/10.2166/wst.2020.326.

[109] N. Gupta, A. Shrivastava, R.K. Sharma, Silica nanoparticles coencapsulating gadolinium oxide and horseradish peroxidase for imaging and therapeutic applications, Int. J. Nanomedicine 7 (2012) 5491–5500, https://doi.org/10.2147/IJN.S33295.

[110] N. Gupta, C. Gupta, S. Sharma, B. Rathi, R.K. Sharma, H.B. Bohidar, Magnetic iron oxide nanoparticles encapsulating horseradish peroxidase (HRP): synthesis, characterization and carrier for the generation of free radicals for potential applications in cancer therapy, RSC Adv. 6 (2016) 111099–111108, https://doi.org/10.1039/C6RA24586B.

[111] A.A. Date, J. Hanes, L.M. Ensign, Nanoparticles for oral delivery: design, evaluation and state-of-the-art, J. Control. Release 240 (2016) 504–526, https://doi.org/10.1016/j.jconrel.2016.06.016.

[112] H.H. Huang, S.M. Kuo, Y.J. Wu, J.H. Su, Improvement and enhancement of antibladder carcinoma cell effects of heteronemin by the nanosized hyaluronan aggregation, Int. J. Nanomedicine 11 (2016) 1237–1251, https://doi.org/10.2147/IJN.S99911.

[113] Y. Xu, S. Asghar, L. Yang, Z. Chen, H. Li, W. Shi, Y. Li, Q. Shi, Q. Ping, Y. Xiao, Nanoparticles based on chitosan hydrochloride/hyaluronic acid/PEG containing curcumin: In vitro evaluation and pharmacokinetics in rats, Int. J. Biol.

Macromol. 102 (2017) 1083–1091, https://doi.org/10.1016/j.ijbiomac.2017.04.105.
[114] M.L. Bruschi, Mathematical models of drug release. Strategies to Modify the Drug Release From Pharmaceutical Systems, Woodhead Publishing, 2015, pp. 63–86, https://doi.org/10.1016/b978-0-08-100092-2.00005-9.
[115] D. Wójcik-Pastuszka, J. Krzak, B. Macikowski, R. Berkowski, B. Osiński, W. Musiał, Evaluation of the release kinetics of a pharmacologically active substance from model intra-articular implants replacing the cruciate ligaments of the knee, Materials (Basel). 12 (2019), https://doi.org/10.3390/ma12081202.
[116] R. Gouda, H. Baishya, Z. Qing, Application of mathematical models in drug release kinetics of Carbidopa and levodopa ER tablets, J. Dev. Drugs 06 (2017) 1–8, https://doi.org/10.4172/2329-6631.1000171.
[117] X. Cao, C. Chen, H. Yu, P. Wang, Horseradish peroxidase-encapsulated chitosan nanoparticles for enzyme-prodrug cancer therapy, Biotechnol. Lett. 37 (2015) 81–88, https://doi.org/10.1007/s10529-014-1664-5.